



HAL
open science

Modulation of the expression and activity of cathepsin S in reconstructed human skin by neohesperidin dihydrochalcone

J. Sage, J. Renault, R. Domain, K.K. Bojarski, T. Chazeirat, A. Saidi, E.
Leblanc, C. Nizard, S.A. Samsonov, R. Kurfurst, et al.

► To cite this version:

J. Sage, J. Renault, R. Domain, K.K. Bojarski, T. Chazeirat, et al.. Modulation of the expression and activity of cathepsin S in reconstructed human skin by neohesperidin dihydrochalcone. *Matrix Biology*, 2022, 107, pp.97-112. 10.1016/j.matbio.2022.02.003 . hal-03677291

HAL Id: hal-03677291

<https://hal.science/hal-03677291v1>

Submitted on 22 Jul 2024

HAL is a multi-disciplinary open access archive for the deposit and dissemination of scientific research documents, whether they are published or not. The documents may come from teaching and research institutions in France or abroad, or from public or private research centers.

L'archive ouverte pluridisciplinaire **HAL**, est destinée au dépôt et à la diffusion de documents scientifiques de niveau recherche, publiés ou non, émanant des établissements d'enseignement et de recherche français ou étrangers, des laboratoires publics ou privés.



Distributed under a Creative Commons Attribution - NonCommercial 4.0 International License



Modulation of the expression and activity of cathepsin S in reconstructed human skin by neohesperidin dihydrochalcone



J. Sage^{a,*}, J. Renault^{b,c,*}, R. Domain^{b,c}, K.K. Bojarski^d, T. Chazeirat^{b,c}, A. Saidi^{b,c}, E. Leblanc^a, C. Nizard^a, S.A. Samsonov^d, R. Kurfurst^a, G. Lalmanach^{b,c} and F. Lecaille^{b,c}

a - LVMH-Recherche, Saint Jean de Braye F-45800, France

b - Université de Tours, Tours, France

c - INSERM, Centre d'Etude des Pathologies Respiratoires, Team Mécanismes Protéolytiques dans l'Inflammation, UMR 1100, Tours F-37032, France

d - Faculty of Chemistry, University of Gdańsk, Gdańsk 80-308, Poland

Corresponding to Fabien Lecaille: Fabien Lecaille, Université de Tours, INSERM, UMR 1100, CEPR, 10 Boulevard Tonnellé, F-37032 Tours cedex, France. fabien.lecaille@univ-tours.fr
<https://doi.org/10.1016/j.matbio.2022.02.003>

Abstract

Dysregulation of cathepsin S (Cat S), a cysteine protease involved in extracellular-matrix and basement membrane (BM) degradation, is a concomitant feature of several inflammatory skin diseases. Therefore, Cat S has been suggested as a potential therapeutic target. Flavonoids, which were identified as regulatory molecules of various proteolytic enzymes, exert beneficial effects on skin epidermis. Herein, thirteen flavonoid compounds were screened *in vitro* and *in silico* and neohesperidin dihydrochalcone (NHDC) was identified as a potent, competitive, and selective inhibitor ($K_i=8\pm 1 \mu\text{M}$) of Cat S. Furthermore, Cat S-dependent hydrolysis of nidogen-1, a keystone protein of BM architecture, as well as elastin, collagens I and IV was impaired by NHDC, while both expression and activity of Cat S were significantly reduced in NHDC-treated human keratinocytes. Moreover, a reconstructed human skin model showed a significant decrease of both mRNA and protein levels of Cat S after NHDC treatment. Conversely, the expression of nidogen-1 was significantly increased. NHDC raised IL-10 expression, an anti-inflammatory cytokine, and mediated STAT3 signaling pathway, which in turn dampened Cat S expression. Our findings support that NHDC may represent a valuable scaffold for structural improvement and development of Cat S inhibitors to preserve the matrix integrity and favor skin homeostasis during inflammatory events.

© 2022 Elsevier B.V. All rights reserved.

Introduction

Human cathepsin S (Cat S, EC 3.4.22.27) is a non-glycosylated lysosomal papain-like cysteine protease that is primarily expressed in many antigen presenting cells (dendritic cells, macrophages, and B cells) and participates in MHC-II antigen presentation (for review: [1]). In addition, Cat S is found in a range of resident cells including keratinocytes, and its expression can be induced by pro-inflammatory stimuli. Among the members of human cysteine cathepsin family (cathepsins B, C, H, F, K, L, O, S, V, W, and X), Cat S has the unique property to be

highly active and stable at neutral pH, supporting its potential involvement in extracellular proteolytic activities [2,3]. Moreover, some cells (i.e., macrophages, osteoclasts, tumor cells) express vacuolar-type H^+ -ATPase pumps that lower the pericellular pH, thus subsequently triggering cysteine cathepsin activity [4–7]. Accordingly, Cat S participates in matrix remodeling by the degradation at acidic and neutral pH of extracellular matrix (ECM) constituents such as elastin and collagen type I, as well as basement membrane (BM) components, including laminins, collagen type IV, and nidogen-1 (nid-1) [8–10]. More specifically, beside other proteases (e.g.

MMP-1, -3, -9, elastase, cysteine cathepsins B, K, L, and V), Cat S contributes to highly specific intra- and extracellularly proteolytic processes in human skin, supporting that Cat S represents a major regulator of barrier function and immune homeostasis [11,12]. Aberrant expression and activity of Cat S is related to the pathogenesis of autoimmune diseases in skin (e.g. psoriasis, atopic dermatitis), highlighting its potential as an attractive therapeutic target [13–21].

Beside synthetic chemicals, it is now well admitted that numerous natural compounds with high bioavailability and low cytotoxicity can provide a wide range of potential health benefits. Flavonoid compounds, which are extensively present in the kingdom of plants, have sparked great attention in recent years, considering their potent antioxidant, metal chelation, anti-inflammatory, antimicrobial, antifungal, anticancer, and antiviral properties (for review: [22]). Moreover, flavonoids exert powerful anti-aging and photoprotective effects on the skin through the regulation of various proteolytic enzyme types, including metallo-, serine, aspartic proteases as well cysteine cathepsins B, H, K, L, and V (for review: [23]). Despite their ability to inhibit Cat S has never been investigated, flavonoids may represent promising candidates to modulate Cat S extracellular activity and to preserve BM integrity at the dermal epidermal junction (DEJ). Therefore, this work aimed to analyze the ability of five representative chemical classes of thirteen commercial flavonoids including flavones (chrysin and apigenin), flavanones (naringenin, hesperitin, eriodictyol, neohesperidin), flavanols (gallocatechin, neohesperidin epigallocatechin 3-gallate), flavonols (myricetin, quercetin, kaempferol), and dihydrochalcones (cardamonin, neohesperidin dihydrochalcone) to inhibit Cat S activity. Among these compounds, neohesperidin dihydrochalcone (NHDC) displayed the most potent inhibitory activity against Cat S. The mechanism of inhibition was determined by *in vitro* kinetics analysis, and interactions between Cat S and NHDC were evaluated *in silico* by molecular docking. Moreover, consequences of NDHC-dependent Cat S inhibition on keratinocytes and a reconstructed human skin (RHS) model were examined as well the signaling pathway underlying the modulation of Cat S expression. Our results suggested that NHDC may provide an effective scaffold for development of specific and selective small Cat S inhibitors as skin therapeutic agents, which could be further exploited in topical formulations during inflammatory skin disorders.

Results and discussion

Screening of flavonoids for inhibitory activity against Cat S

Except epigallocatechin 3-gallate (EGCG) and to a less extent kaempferol and cardamonin, all tested

compounds showed some dose-dependent inhibitory effect toward Cat S activity (Supplementary Fig. 1). Among them, neohesperidin dihydrochalcone (NHDC), was the most potent inhibitor of Cat S-mediated Z-FR-AMC hydrolysis. The inhibition constant (K_i) values were further determined, and results reported in Table 1. NHDC inhibited Cat S according to a reversible mechanism with a K_i of $8 \pm 1 \mu\text{M}$, while neohesperidin (NHP) was less effective with a K_i of $27 \pm 9 \mu\text{M}$, suggesting that linearization of the pyrane ring C (see the nomenclature of chrysin and NHDC structures, Table 1), which leads to a ~ 2.5 -fold increase of the dipolar moment, may assist interactions with the enzyme (Supplementary Table 1). Also, hesperetin, the aglycone form of NHP, had a weaker inhibitory capacity ($K_i = 127 \pm 23 \mu\text{M}$) *in vitro*, suggesting that the substitution of the benzene ring A by a sugar moiety (i.e., 4'-((2-O-[6-Deoxy- α -L-mannopyranosyl]- β -D-glucopyranosyl)oxy)) could favor inhibition of Cat S. The low potency of cardamonin, a chalcone aglycone, to inhibit Cat S ($K_i = 327 \pm 56 \mu\text{M}$) corroborated the likely importance of this structural feature.

Competitive inhibition of Cat S by NHDC

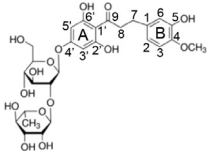
NHDC inhibited Cat S in a competitive manner, since the vertical axis intercept ($1/V_m$) remained while the horizontal axis intercept ($-1/K_m$) increased with NHDC concentration (Fig. 1A). The secondary plot of slopes of Lineweaver-Burk (K_{app}) vs. [NHDC] was linearly fitted (shown in the inset), which indicated that NHDC bound to the substrate binding site of Cat S. Conversely, Cat S inhibition by flavones, flavanones, flavanols and flavonols best corresponded to a non-competitive mechanism (data not shown). Preincubation (0-120 min) of Cat S with NHDC at a concentration eliciting $\sim 50\%$ inhibition of its peptidase activity revealed that Cat S inhibition was highly stable, since $\geq 99\%$ NHDC inhibitory potential was retrieved after 2h-incubation (Fig. 1B). On the other hand, NHDC remained an effective inhibitor of Cat S at pH 7.4 ($K_i = 40 \pm 6 \mu\text{M}$), supporting its potential to reduce extracellularly the proteolysis of ECM components by Cat S. NHDC was also tested at pH 5.5 against closely related human cathepsins L (Cat L) and B (Cat B), which are the two prevalent and ubiquitous papain-like cysteine proteases expressed by keratinocytes in skin epidermis [10,24]. The inhibitory effect of NHDC on both Cat L and Cat B was substantially weaker than that of Cat S, with a ~ 18 -20-fold K_i increase (Cat L: $K_i = 144 \pm 22 \mu\text{M}$, Cat B: $K_i = 167 \pm 11 \mu\text{M}$) assessing a fairly selectivity towards Cat S (Fig. 1C). Moreover, NHDC demonstrated a substantially weaker inhibitory activity ($K_i = 61 \pm 16 \mu\text{M}$) towards the related cathepsin-L like enzyme, human cathepsin K at pH 5.5. Likewise, NHDC inhibited in a dose dependent manner hydrolysis of fluorogenic substrates derived from

Table 1. K_i values for inhibition of Cat S by flavonoids.

	#	Compound	Structure	K_i (μM)
Flavones	1	Chrysin		111±36
	2	Apigenin		96±7
Flavanones	3	Naringenin		109±33
	4	Hesperetin		127±23
	5	Eriodictyol		162±45
	6	Neohesperidin (NHP)		27±9
Flavanols	7	Gallocatechin		86±24
	8	Epigallocatechin 3-gallate (EGCG)		326±22
Flavonols	9	Myricetin		72±10
	10	Quercetin		73±12
	11	Kaempferol		132±37
Dihydrochalcones	12	Cardamonin		327±56

(continued)

Table 1 (Continued)

#	Compound	Structure	Ki (μM)
13	Neohesperidin dihydrochalcone (NHDC)		8±1

Basic flavonoid structure corresponds to a fifteen-carbon skeleton consisting of two benzene rings (A and B as shown in chrysin) linked via a heterocyclic pyrane ring (C).

elastin, collagens type I and IV, supporting that NHDC could effectively impair both elastolytic and collagenolytic activities of Cat S, besides its peptidase activity (Fig. 2). Moreover, proteolysis of nidogen-1 (nid-1), a key protein in BM assembly and a specific substrate of Cat S [10,25], is readily prevented by NHDC (100 μM).

Identification of putative binding sites of NHDC on Cat S

Molecular docking simulations were performed to provide intermolecular insights in the interactions between flavonoids and Cat S. Molecular docking of the thirteen flavonoids predicted binding affinity (ΔG_{calc}) in a similar range for all examined complexes (difference magnitude ± 2 kcal/mol) with a preference in the substrate-binding site (catalytic cavity) of the enzyme (supplementary Table 1). Interestingly, among the flavonoids tested, only chrysin, naringenin, kaempferol, and NHDC were docked exclusively in the active site of Cat S, with NHDC poses in the top-ranking binding scores ($\Delta G_{\text{calc}} = -7.4$ kcal/mol). In addition, docking scores positively correlated with experimental free binding energy (ΔG_{exp}) (Pearson correlation: $r = 0.707$, $p = 0.007$). Principal component analysis (PCA) was then used to identify molecular descriptors of flavonoids that may be important in the inhibition of Cat S. A linear positive relationship ($r = 0.78$, $p = 0.0017$) was established between ΔG_{exp} and the partition coefficient in octanol/water (LogP), while a negative correlation was measured between ΔG_{exp} and polar surface area ($r = -0.66$, $p = 0.014$) (Fig. 3A, B). Moreover, ΔG_{exp} correlated negatively with mass ($r = -0.68$, $p = 0.010$), accessible surface area ($r = -0.68$, $p = 0.01$), H-bond acceptor ($r = -0.69$, $p = 0.008$), and orientable bonds ($r = -0.63$, $p = 0.02$) of tested compounds. Results indicated that large and polar flavonoid compounds with the lowest lipophilicity, i.e., NHDC, constituted the most efficient inhibitors of Cat S. Molecular dynamics (MD) was used to give a better view on stability of NHDC-Cat S complexes than that obtained from molecular docking. As depicted in Fig. 3 C, MD unveiled that NHDC likely bound to the active site rather than other sites located on the protein surface. Indeed, mean values

of five binding free energies obtained from 20 ns MD simulation at pH 7 of NHDC in the active and non-active site were $\Delta G = -24.7 \pm 4$ kcal/mol and $\Delta G = -22.0 \pm 4.5$ kcal/mol, respectively. The competitive inhibition mode of Cat S by NHDC deduced from kinetic studies was consistent with MD analysis. NHDC exhibited a binding pose covering preferentially the central region of the Cat S substrate-binding site, by establishing hydrogen bonds with residues Q19, G23, G65, and G69 (Fig. 3D). Regarding the disaccharide moiety of NHDC (4'-((2-O-[6-Deoxy- α -L-mannopyranosyl]- β -D-glucopyranosyl) oxy), deoxy- α -L-mannopyranose bound preferentially to the S2 pocket of Cat S, while β -D-glucopyranose bound preferentially to the S1 sub-site.

Effect of NHDC on Cat S in human keratinocytes

After assessing that NHDC was a relevant inhibitor of Cat S *in vitro* and *in silico*, we investigated its cellular effects on keratinocytes, the predominant cell type in epidermis (Fig. 4). First, we analyzed the cell viability of normal human epidermal keratinocytes (NHEK), following a treatment by NHDC (0, 100 μM, and 500 μM) for 24 h. No significant cell cytotoxicity at high concentration was measured, and relatively homogenous monolayers of small (10-20 μm) cells were observed in the absence and presence of NHDC (Fig. 4A). These results corroborated previous findings on the safety profile of NHDC on different cell types (fibroblasts, stem cells) [26,27], contrasting to several structurally related polyphenols (i.e., apigenin, naringenin, eriodictyol, kaempferol, quercetin) that exhibited at high concentrations deleterious effect on cell viability of numerous human cells, including HaCaT keratinocytes [28,29]. Then, impact of NHDC on Cat S expression (mRNA, protein) and activity of growing NHEK was evaluated. Both mRNA expression and intracellular protein level were reduced ($p < 0.05$) in cell lysates of NHDC-treated keratinocytes compared with the control group, reaching a ~ 1.6 -fold decrease with 500 μM NHDC (Fig. 4B, C). Consistently, specific enzymatic activity of secreted Cat S, using Z-LR-AMC as substrate, decreased in a dose-dependent manner under treatment with NHDC ($p < 0.001$)

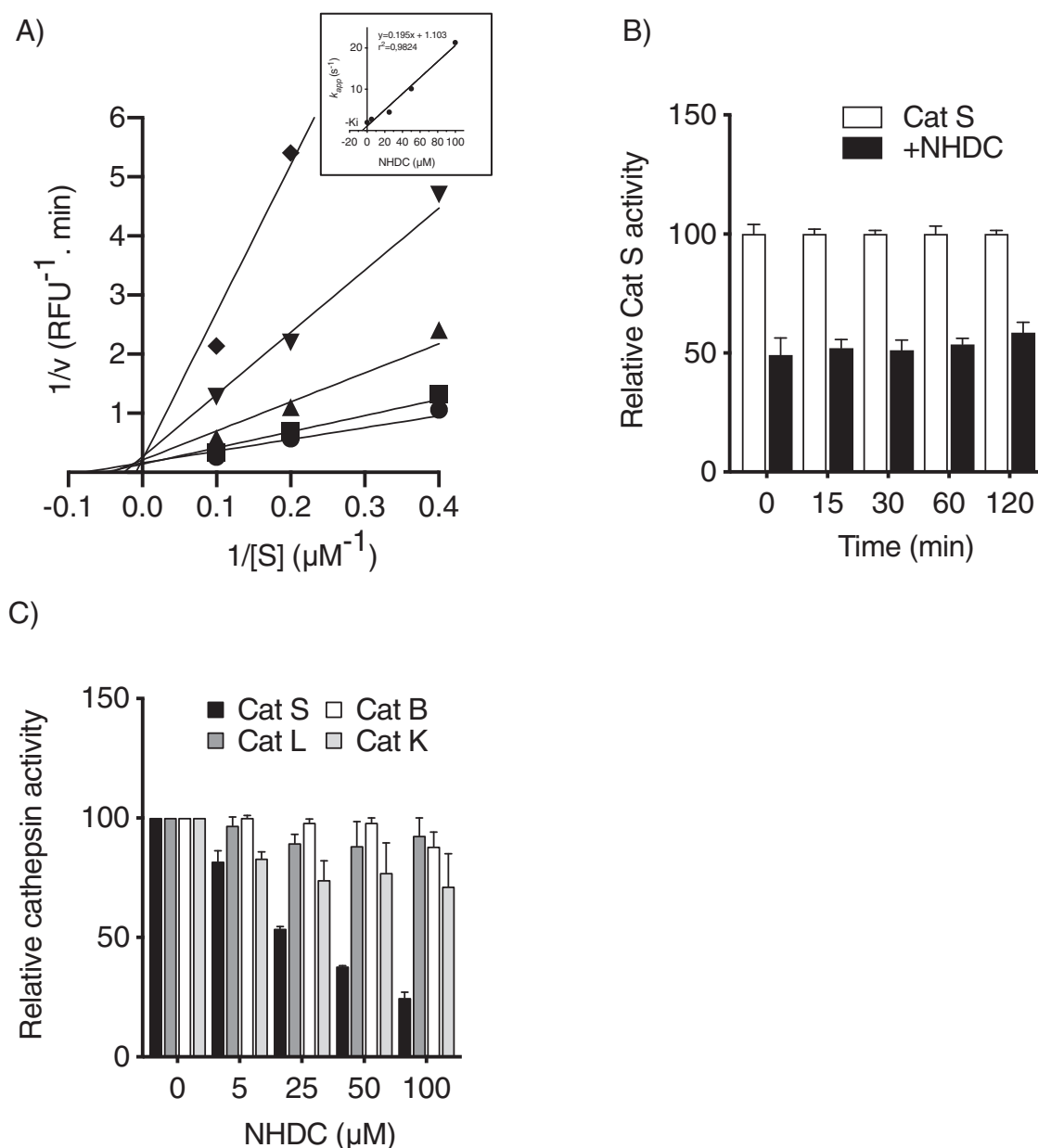


Fig. 1. Competitive and selective inhibition of Cat S by NHDC. A) Lineweaver-Burk plots analysis of Cat S inhibition. To determine the nature of inhibition of Cat S by NHDC, the rate of Cat S (0.2 nM) was measured with Z-FR-AMC at different concentrations in the presence of NHDC (0 μM : \bullet ; 5 μM : \blacksquare ; 25 μM : \blacktriangle ; 50 μM : \blacktriangledown and 100 μM : \blacklozenge). Enzyme activity was expressed as RFU/min (relative fluorescence units of AMC released per unit of time). Results are the mean of 3 experiments conducted in triplicates. The values of K_{app} were calculated by double reciprocal plots at four concentrations of substrate Z-FR-AMC and in presence of five different concentrations of NHDC (insert). Intersection of the slope with x axis corresponds to $-K_i$. B) Stability of NHDC (50 μM) to inhibit Cat S (0.5 nM) at pH 5.5 over time. Cat S activity: data assays were normalized to 100% of the respective value at $t=0$ min, in the absence of NHDC. C) Inhibition of the peptidase activity (Z-FR-AMC: 10 μM) of Cat B, Cat L, Cat K, and Cat S (final concentration: 0.5 nM) with NHDC in the activity buffer (pH 5.5). The activity is expressed as a percentage and compared to the control without NHDC (100% activity).

(Fig. 4D). Data indicated that a relatively short-term (24 h) treatment by NHDC can down regulate Cat S expression in keratinocytes, supporting that NHDC could be a valuable reagent for the regulation of Cat S in inflammatory responses. These findings

prompted us to explore whether a long-term treatment with NHDC might unveil a direct inhibitory effect on the Cat S expression in skin, consequently associated to a reduction in the remodeling and/or degradation of matrix (BM and ECM) components.

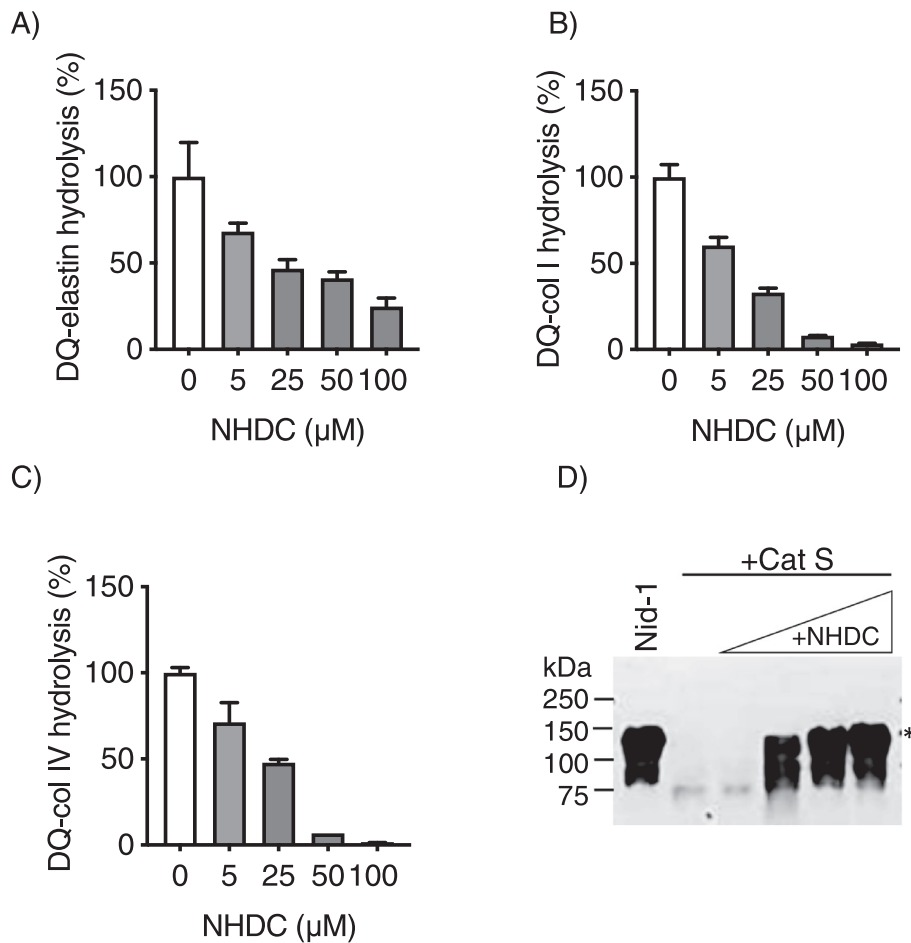


Fig. 2. Inhibition of the proteolytic activity of Cat S by NHDC. Cat S (0.5 nM) was incubated in the activity buffer pH (5.5) in the absence and presence of NHDC (5, 25, 50, and 100 μM). Collagenase and elastase activities of Cat S were measured with the following fluorogenic substrates: A) DQ-elastin (10 μg/mL), B) DQ-collagen I (10 μg/mL), C) DQ-collagen IV (10 μg/mL). The activity was expressed as a percentage and compared to the control without NHDC (100% activity). Results are expressed as mean ± standard deviation (SD) of three independent experiments, each performed in duplicate. D) Representative western-blot of nidogen-1 (nid-1, 50 ng) incubated 30 min in the activity buffer (pH 5.5) or in the presence of Cat S (10 nM) with increasing concentrations of NHDC (from left to right: 1 μM, 50 μM, 100 μM, and 200 μM). Star indicates the location of nid-1.

Effect of NHDC on Cat S and matrix components in reconstructed human skin (RHS) model

A biologically relevant model of reconstructed human skin (RHS) consisting of an epidermis and dermis separated by a basement membrane (BM) and populated with human skin cells (keratinocytes and fibroblasts) was previously developed [30]. Accordingly, RHS could represent an appropriate template to identify and characterize changes in Cat S expression and BM protein integrity following exposure to NHDC (100 μM) for 14 days. Histological examination revealed a completely stratified epithelium in *de novo* RHS, which closely resembled normal human epidermis (Fig. 5A). Immunostaining of RHS cryosections with anti-human Cat S antibodies revealed that Cat S, which was broadly

expressed in epidermis and to a lesser extent in dermis, was significantly reduced in NHDC-treated RHS compared to control (Fig. 5B), consistent with the observed decrease in Cat S levels in NHDC-treated keratinocytes. Conversely, a noticeable change in the amount of specific BM constituents was observed. A significant increase of nid-1 and laminin-1, but not collagen type IV was measured in the dermal epidermal junction (DEJ) of NHDC-treated RHS. In addition, immunohistochemistry (IHC) analysis of ECM proteins in dermis revealed that elastin, fibronectin, and collagen type I staining was significantly increased after 14 days of NHDC treatment (Fig. 5B), while collagen type VII, and fibrillin levels were unchanged (data not shown). IHC results for both Cat S and nid-1 were confirmed by sandwich ELISA in RHS lysates (Fig. 5C). One

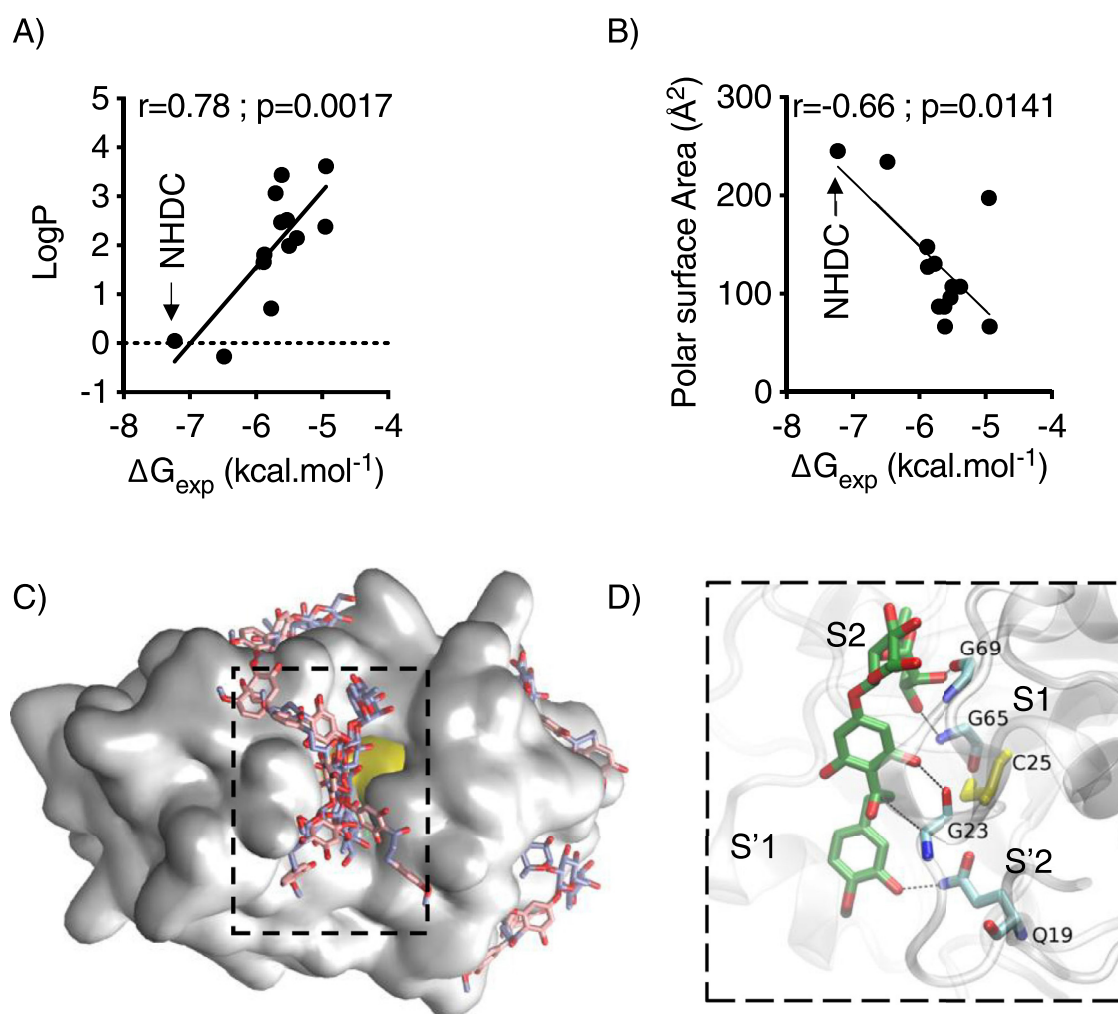


Fig. 3. Docking model of NHDC with Cat S. A) Experimental Gibbs free energy (ΔG_{exp}) of the thirteen flavonoids were plotted against partition coefficient (LogP). ΔG_{exp} was obtained from experimental K_i , using the formula $\Delta G = R.T.\ln(K_i)$. B) Correlation between polar surface area and ΔG_{exp} . The significance of the correlation was assessed with Pearson coefficient (r). C) Top 10 dock poses of NHDC (pink and cyan sticks) on Cat S (light grey surface) with a focus of the active site (dotted square). Cysteine 25 (C25) of the catalytic site is depicted in yellow. D) Hydrogen bonds between NHDC (green sticks) and residues Q19, G23, G65, and G69 of the active cleft of Cat S are shown. Subsites S2, S1, S'1, and S'2 are depicted.

can suggest that the increased or unchanged expression of these matrix components, identified as biologically relevant targets of Cat S, can be attributed in part to the decrease of expression/activity of the enzyme by NHDC. Whether downregulation of Cat S secretion is directly triggered by NHDC or depends on other matrix-degrading enzymes will require further investigation.

NHDC exposure altered Cat S expression in RHS through IL-10/STAT3 axis

NHDC, like other flavonoid compounds, encompasses anti-inflammatory effects in various human cells by modulating the expression and secretion of cytokines [31–34]. Furthermore, there is some

evidence that specific cytokines regulate Cat S expression [35]. Accordingly, previous studies reported that interferon-gamma (IFN- γ), a pro-inflammatory cytokine, induces selectively Cat S expression in keratinocytes [13,24], while exposure to interleukin IL-10, a potent anti-inflammatory cytokine, downregulates its expression in macrophages [36]. To further confirm whether the production of these two crucial cytokines is dysregulated in NDHC-treated RHS, we performed a multiplex cytokine analysis. Following NHDC (100 μM) treatment for 14 days, RHS supernatants showed a significant increased release of IL-10 (40.49 ± 2.92 pg/mL) compared to control groups (28.01 ± 2.70 pg/mL), while NHDC successfully reduced expression of IFN- γ ($p=0.011$) (Fig. 5C). In the same line, NHDC (100

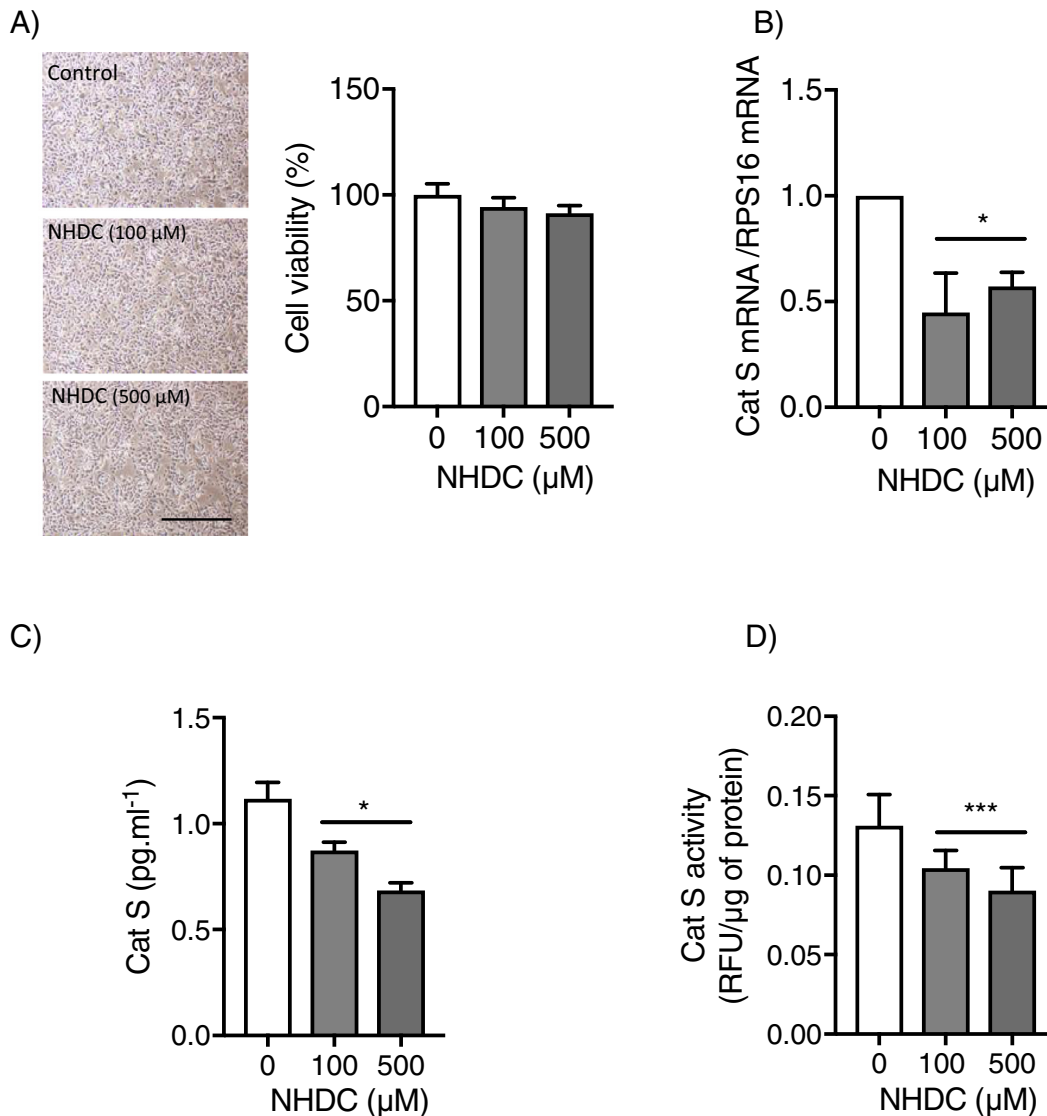


Fig. 4. Effect of NHDC on Cat S expression/activity in human keratinocytes. A) General morphology of normal human epidermal keratinocytes (NHEK) grown during 24 h in the absence (control) or with NHDC (100 and 500 μM). Cells in monolayer culture were photographed using light microscopy (scale bar: 200 μm). Cell viability of NHDC was performed by WST-1 assays ($n=3$). Data are expressed as a percentage and compared to the control without NHDC (100%). B) Cat S mRNA levels were analyzed by RT-qPCR and normalized to the levels of RPS16 mRNA. C) Cat S protein levels (ELISA) in NHEK lysates, ($n=3$, duplicate). D) Cat S activity in cell-free supernatants. Supernatants were pretreated in the presence of proteases inhibitors cocktail. Cat S activity (relative fluorescence unit: RFU) in supernatant (30 μg of protein deposited) was monitored using Z-Leu-Arg-AMC (30 μM) ($n=3$, duplicate) (see material and methods for details). Error bars represent median values \pm S.D. Statistical significance was assessed between NHDC-treated cells and non-treated cells using the non-parametric Mann-Whitney U-test (* $P < 0.05$; *** $P < 0.001$).

μM) did not alter pro-inflammatory cytokine IL-6 secretion, as reported elsewhere in LPS-stimulated murine macrophages model [31] (Supplementary Fig. 2A). A similar result was observed for IL-8 (Supplementary Fig. 2B). In addition to suppress IFN- γ signaling, a previous report indicated that IL-10 activates its primary mediator, signal transducer and activator of transcription 3 (STAT3), concomitantly with the down expression of Cat S in human

macrophages [36]. To examine whether NHDC could upregulate STAT3 in epidermis, we performed western-blot analysis on untreated and NHDC-treated RHS lysates. As shown in Fig. 5D, treatment with NHDC triggered STAT3 phosphorylation (P-STAT3). Conversely, activation of STAT3 led to a marked decrease in Cat S protein levels in NHDC-treated RHS lysates, corroborating ELISA experiments (Fig. 5C). Taken together, this result

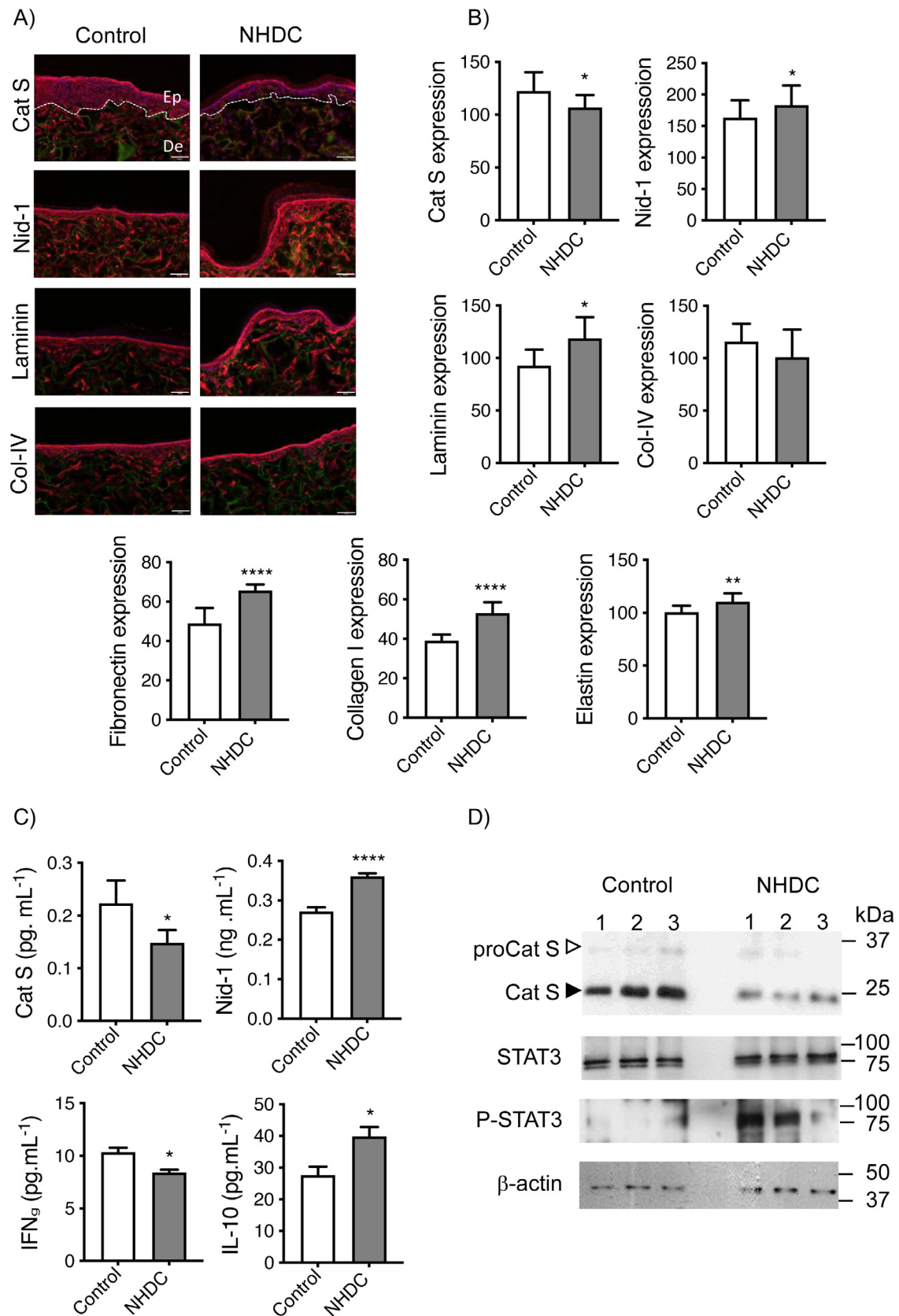


Fig. 5. Effect of NHDC on Cat S and BM components expression in reconstructed human skin. A) Representative image of immunofluorescence staining of Cat S, nidogen-1, laminin-332/511, and collagen-IV in reconstructed human

supported that the downregulation of Cat S by NHDC in RHS is associated with the IL-10/STAT3 axis. Nevertheless, it cannot be excluded that NHDC could also interfere with other potential cellular pathways involved in the regulation of cathepsin expression.

Conclusions

Over the last 20 years, extensive efforts have been devoted to the search and the development of synthetic or natural derivative inhibitors of Cat S, leading to the discovery of potent and selective covalent and non-covalent inhibitors (for review: [37]). However, no study has investigated the inhibitory potency of the flavonoids on Cat S, contrary to its counterparts cathepsins B, L, K, and V (for review: [23]). In the present work, among thirteen commercial flavonoids from five chemical subclasses, we identified NHDC as a potent reversible and competitive inhibitor of Cat S at both acidic and neutral pH. Moreover, NHDC displayed a reasonable selectivity for Cat S vs human Cat B and Cat L at acidic pH. *In silico* analysis supported kinetics data and suggested that NHDC interacted within the active site of Cat S by establishing hydrogen bonds. Electrostatic and van der Waals interactions may also contribute to the overall binding affinity of NHDC toward Cat S.

Based on prior studies supporting that NHDC has no toxicity on cells and animals [38,39], we examined the consequences of exposure of human keratinocytes to NHDC on Cat S expression and the impact of Cat S inhibition in a reconstructed human skin (RHS) model. Treatment of keratinocytes and RHS with NHDC resulted in a significant reduction of Cat S expression, whereas levels of major ECM and BM constituents in epidermis (i.e. nid-1, laminin-1, elastin, fibronectin, and collagen type I), were noticeably increased. Moreover, Cat S downregulation is associated to IL-10-induced STAT3 activation, as previously reported in primary human blood macrophages [36]. Accordingly, the Fig. 6 summarizes a putative signaling pathway in epidermis. Alternatively, NHDC may also have an indirect effect of cathepsin S expression by modulating other cofactors and cellular mechanisms. For instance,

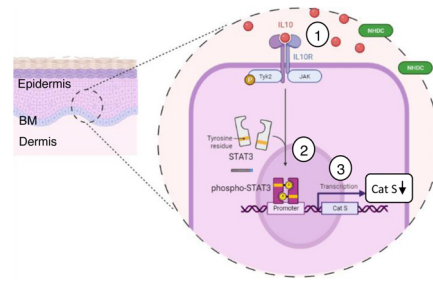


Fig. 6. Putative model of NHDC-induced down expression of Cat S in human skin. We propose that NHDC induces the production of IL-10 (1), which binds to its receptor and subsequently activates STAT3 (2). Phosphorylation of STAT3 downregulates Cat S expression (3). Figure was created by BioRender.com. BM: basement membrane.

Cat S may be secreted via secretory lysosomes upon elevation of intracellular Ca^{2+} levels, which favors its release into the extracellular space [40]. Interestingly, some natural flavonoids change the intracellular Ca^{2+} homeostasis linked to functional alterations of the mitochondria, Ca^{2+} channels and Ca^{2+} pumps [41], supporting that NHDC may also modify calcium homeostasis. Accordingly, analysis of the regulation of Ca^{2+} by NHDC could be the purpose of further study. Finally, besides its antioxidative, anti-inflammatory, and anti-apoptotic properties [34], NHDC may have therapeutic activity by reducing Cat S expression/activity during skin inflammatory diseases. Conceivably, NHDC could be used as a lead framework for the further development of a more specific and selective Cat S inhibitor to prevent dysregulated ECM and BM proteolysis mediated by overexpressed Cat S during skin diseases, including psoriasis and atopic dermatitis.

Experimental procedures

Enzymes, substrates, and inhibitors

All the chemicals were of analytical grade. Human cysteine cathepsins B, L, and S were supplied by Calbiochem (VWR International S.A.S., France) and their active site titration was determined using L-3-carboxy-trans-2, 3-epoxy-propionylleucylamide-(4-guanido)-

skin (RHS) model. RHS were cultivated 14 days in the absence (control, n=3) or with NHDC (100 μ M, n=3). Scale bar = 100 μ m. B) Following confocal laser microscopy acquisition pictures (four randomly chosen areas from each RHS) were analyzed, and relative expression of Cat S was quantified and standardized to the epidermis surface. Quantification of basement membrane proteins expression was standardized to the dermal-epidermal junction surface. Relative expression of fibronectin, collagen type I, and elastin was quantified and standardized to the dermis surface. C) The cell culture from RHS was analyzed for Cat S, nidogen-1 content (lysates), and cytokines (supernatants) using dedicated ELISA kits. Data represent the mean \pm S.D. D) Western blot analysis of Cat S, STAT3, and P-STAT3 in lysates of three RHS treated or not with NHDC. β -actin served as a loading control. Data are representative of at least three biological independent repeats. (* p <0.05; ** p <0.01; **** p <0.0001). Epidermis (Ep), dermal-epidermal junction (dashed line), and dermis (De).

butane (E-64) (Sigma-Aldrich, Saint-Quentin Fallavier, France). Human cathepsin K was produced as described elsewhere [42]. 7-amino-4-methylcoumarin (AMC) was supplied by Sigma-Aldrich, while peptidyl-AMC substrates: Z-FR-AMC and Z-LR-AMC (benzyloxycarbonyl-Phe/Leu-Arg-7-amino-4-methyl coumarin) came from R&D System (Abingdon, UK). Activity assays were performed in the following buffer: 100 mM acetate sodium buffer, pH 5.5, 2 mM dithiothreitol (DTT), and 0.01% Brij35 or in 100 mM Hepes buffer, pH 7.4, 2 mM DTT, and 0.01% Brij35. Enzymatic assays were carried out at 37°C in the activity buffer, using Z-FR-AMC or Z-LR-AMC ($\lambda_{\text{ex}}=350$ nm, $\lambda_{\text{em}}=460$ nm). DQ-elastin, DQ-collagen types I and IV were purchased from Molecular Probes (Life Technologies, Saint Aubin, France). Elastinolytic and collagenolytic assays were monitored using a 96-well microplate reader spectrofluorometer (SpectraMax Gemini, Molecular Devices, Saint Gregoire, France) ($\lambda_{\text{ex}}=495$ nm, $\lambda_{\text{em}}=515$ nm). Recombinant human nidogen-1 was from R&D System. Pepstatin A, ethylene diamine tetraacetic acid (EDTA), AEBSF (Pefabloc), and S-methyl thiomethanesulfonate (MMTS) were from Sigma-Aldrich. Morpholinourea-leucinyl-homophenylalanine-vinyl-sulfone phenyl inhibitor (LHVS) was provided by Dr. J. H. McKerrow (Skaggs School of Pharmacy and Pharmaceutical Sciences, University of California, San Diego, USA).

Flavonoids

Thirteen flavonoids were provided by Sigma-Aldrich (purity > 95%) including chrysin (MW: 254.24 g/mol), apigenin (MW: 270.24 g/mol), naringenin (MW: 272.25 g/mol), hesperetin (MW: 302.28 g/mol), eriodictyol (MW: 288.25 g/mol), neohesperidin (NHP) (MW: 610.56 g/mol), gallicocatechin (MW: 306.27 g/mol), epigallocatechin 3-gallate (EGCG) (MW: 458.37 g/mol), myricetin (MW: 318.24 g/mol), quercetin (MW: 302.24 g/mol), kaempferol (MW: 286.24 g/mol), cardamonin (270.28 g/mol), and neohesperidin dihydrochalcone (MW: 612.58 g/mol).

Enzyme inhibition studies

First, Cat S (0.2 nM) was incubated with each flavonoid (0-100 μM) in the activity buffer (pH 5.5) at 37°C for 10 min to screen their potent inhibitory potency. After addition of Z-FR-AMC (10 μM) the residual enzymatic activity of Cat S was followed by monitoring the fluorescence release of AMC. The experiments were performed in triplicate for each concentration. Then, Cat S (0.5 nM) was incubated with each flavonoid (0-100 μM) in the activity buffer (pH 5.5) at 37°C for 10 min before adding various amount of Z-FR-AMC (1-10 μM) to determine the type of inhibition. All assays were carried out in triplicate for each concentration of flavonoid and averaged before further calculations. Inhibition constant

(K_i) values were calculated using Lineweaver-Burk plots, plotting $1/v$ against $1/Z\text{-FR-AMC}$. The K_i value for NHDC was also determined at pH 7.4 for Cat S and at pH 5.5 for Cat L, Cat B, and Cat K. The data were further analyzed by Dixon plots ($1/v=f(\text{flavonoid})$) and non-linear regression analyses to ascertain the modality of inhibitor binding (GraphPad Prism, San Diego, CA, USA).

Correction of fluorescence quenching in Cat S kinetics

Considering the overlay of absorbance wavelength of AMC-derived substrates and some flavonoids (apigenin, eriodictyol, EGCG, myricetin, quercetin, and kaempferol), their effect on fluorescence release was corrected by plotting standard fluorescence curves of free AMC (1-10 μM) in the presence of flavonoid at the concentrations used in our assays. Quenching values were expressed as percent decrease in the AMC fluorescent signal and were calculated using the formula: $(100 - ((F_1/F_0) \times 100))$ (with F_1 =fluorescence of the AMC group in the presence of the flavonoid and F_0 =fluorescence of the AMC group in the absence of the flavonoid). The other flavonoids had negligible effect on the fluorescence of AMC.

Hydrolysis of ECM and BM-derived components by Cat S in the presence of NHDC

Elastinolytic and collagenolytic activities of Cat S (0.5 nM) were measured with the following fluorogenic substrates DQ-collagen I (10 $\mu\text{g}/\text{mL}$), DQ-collagen IV (10 $\mu\text{g}/\text{mL}$), and DQ-elastin (10 $\mu\text{g}/\text{mL}$) in the absence and presence of NHDC (5-100 μM). Alternatively, nidogen-1 (50 ng protein) was incubated with Cat S (10 nM) in the presence of increasing concentrations of NHDC (1-200 μM) in the activity buffer (pH 5.5) for 30 min at 37°C. Samples were separated by SDS-PAGE (10%) and transferred to nitrocellulose membranes for nidogen-1 immunodetection according to [10].

Molecular docking

Flavonoids were modelled with the use of Avogadro software [43] (Hanwell et al., 2012). Charges and geometry parameters required for molecular dynamics (MD) simulations were calculated with the antechamber module of AMBER16 [45]. Molecular docking of flavonoids was performed to Cat S (PDB: 2C0Y) using Autodock Vina, with default parameters and a grid box covering the entire enzyme [44]. The 10 top docked poses were further analyzed. The standard Gibbs free energy (ΔG) change of binding for flavonoids to Cat S was calculated from the experimental values using the following equation: $\Delta G = R.T.\ln(K_i)$. Principal Component Analysis (PCA)

for flavonoids was performed with the KNIME software with a linear regression model [46], using the following parameters: mass, accessible surface area, charge, dipole moment, number of aromatic rings, number of hydrogen bonds donors, acceptors, partition coefficient, solubility, number of rotatable bonds, dissociation constant, polar surface area, and normalized number of hydrogen bonds). Twenty nanosecond MD simulations and free energy calculations were performed using the protocols as described [47].

Ethic statements

Cells were isolated from skin samples collected from patients undergoing surgery and were considered as “waste” and thus were exempt from ethical approval. Helsinki principles were adhered to, and participants gave written, informed consent to provide samples for research.

Cell culture

Normal human epidermal keratinocytes (NHEK) were isolated from abdominal skin of healthy donor (26 years) undergoing abdominal plastic surgery, as described elsewhere [48]. NHEK were grown to 90% confluence in keratinocyte serum-free medium (KFSM, Invitrogen, Cergy Pontoise, France) supplemented with epidermal growth factor (EGF, 5 ng/mL, Invitrogen), bovine pituitary extract (50 mg/mL, Invitrogen), penicillin (100 U/mL, Invitrogen) and streptomycin (100 U/mL, Invitrogen) at 37°C in a 5% CO₂ atmosphere. After determination of non-cytotoxic doses by a viability test (Premix WST-1 Cell Proliferation Assay, Takara Bio Inc, Kusatsu, Japan), keratinocytes were treated or not with NHDC (100, 500 μM) for 24 h. Supernatants and cells were harvested in a preservative buffer (100 mM sodium acetate buffer, pH 5.5, 0.5 mM Pefabloc SC, 0.5 mM EDTA, 1 mM MMTS and 0.04 mM pepstatin A) and stored at -80°C. The protein concentrations in supernatants and cell lysates were determined with the bicinchoninic acid assays kit (BCA protein assay kit, Interchim, Montluçon, France).

Reconstructed human skin (RHS) model

Normal human fibroblasts, isolated from the foreskin of a one-year-old donor, were seeded onto a dermal substrate made of collagen-matrix (Integra LifeSciences, Princeton, NJ, USA). This dermal equivalent was grown for 20 days at 37°C in a 5% CO₂ atmosphere in Dulbecco's modified Eagle's medium (DMEM with Glutamax-1, Life Technologies, Cergy Pontoise, France) supplemented with 10% fetal bovine serum (FBS) (Sigma-Aldrich), 50 μg/mL streptomycin, 50 U/mL penicillin and 1 μg/mL amphotericin B (Life Technologies). The fibroblast

media was supplemented with 50 μg/mL L-ascorbic acid (Sigma-Aldrich) and changed every day. On day 20, normal human keratinocytes (from the same donor as for fibroblasts) were seeded on the dermal equivalent and were grown in a proprietary keratinocyte-media as previously reported [30], and changed every day. After three days of submerged culture, RHS were elevated at the air-liquid interface and cultured in defined keratinocyte serum-free medium changed every two days. On day 27, RHS were treated in the absence or presence of NHDC (100 μM) in simplified keratinocyte medium, with a renewal of treatment every 48 h for two weeks. At the end of the experiment, on day 41, supernatants were collected for further cytokines assays and stored at -80°C. One-half of RHS (n=3 per condition) was harvested for immunohistology studies, while the other half was harvested to proceed to protein extraction. Briefly, RHS were homogenized in cold buffer containing 10 mM Hepes/KOH, pH 7.9, 10 mM KCl, 2 mM MgCl₂, 0.1 mM DTT, 0.1% (v/v) Nonidet P40, in presence of protease inhibitors cocktail (0.5 mM Pefabloc SC, 0.5 mM EDTA, 1 mM MMTS, 0.04 mM pepstatin A). After centrifugation (12,000 x g) during 2 min, supernatants were collected and stored at -80°C. The protein concentrations in cell-free supernatants of RHS were determined with the bicinchoninic acid assays kit.

Antibodies

For western-blot studies, anti-Cat S and anti-nidogen-1 antibodies were from R&D Systems (Minneapolis, MN, USA) (dilution 1:1,000). Anti-β-actin (1:1,000) was from R&D Systems. Anti-STAT3 (1:1,000) was from BD Biosciences (Le Pont de Claix, France). Anti-phospho-STAT3 (Tyr705, 1:1,000) was from Cell Signaling Technology Europe (Leiden, The Netherlands). For immunofluorescence studies, anti-Cat S and anti-nidogen-1 antibodies were diluted 1:100 and 1:250, respectively. Anti-collagen type I, anti-collagen type IV, and anti-elastin antibodies (1:500) were from Novotec (Reuver, Netherlands). Anti-laminin-1 and anti-fibrillin-1 antibodies (1:200) were from ThermoFisher Scientific (Fremont, CA, USA). Anti-fibronectin (1:500) was from Abcam (Cambridge, UK). The secondary antibodies used for WB (1:5,000) and IF (1:200) were respectively from R&D Systems and Life technologies (ThermoFisher Scientific).

Multiplex cytokines, Cat S and nidogen-1 quantification in RHS

Levels of IL-6, IL-8, IL-10 and IFN-γ in RHS supernatants were quantified using the MILLIPIX Multi-Analyte Profiling (MAP) Human Cytokine/Chemokine assay kit (HCYTOMAG-60K, Millipore) and MAGPIX Multiplexing System (Luminex Corporation, Austin,

TX, USA) according to the manufacturer's instructions. Data were analyzed using xPONENT 4.2 software. Cat S and nidogen-1 were quantified using sandwich ELISA DuoSet kits (R&D Systems).

Immunofluorescence in RHS: RHS were embedded in tissue freezing medium (Leica, Wetzlar, Germany) and stored at -80°C before being cut with a cryostat in sections of $20\ \mu\text{m}$ thickness, and analyzed as previously reported [25]. Briefly, quantification of Cat S was standardized to the epidermis surface. Quantification of basement membrane proteins (nid-1, laminin-1, and collagen type IV) was standardized to the dermal-epidermal junction surface. Elastin, collagen type I, fibronectin, and fibrillin quantification were standardized to the dermis surface (Leica QWin digital image processing and analysis software).

Expression and activity of Cat S in NHEK and RHS model: Total RNAs were extracted from NHEK using RNA purification kit (Macherey-Nagel, Hoerd, France) according to the manufacturer's instructions. cDNA was synthesized using $0.5\ \mu\text{g}$ of RNA and RevertAid reverse transcriptase (Thermo Fisher Scientific). The relative transcript expression of Cat S was measured with the LightCycler 480 system (Roche Diagnostics GmbH, Mannheim, Germany) using specific primers [25] and the Powerup SYBR green master mix (Thermo Fisher Scientific). For quantification of relative expression levels, the $\Delta\Delta\text{Ct}$ method was used (normalization gene, human ribosomal protein S16 (RPS16)). The protein concentration of Cat S in NHEK supernatants and lysates, and in RHS lysates were performed using a sandwich ELISA DuoSet kit (R&D Systems). Following running of RHS cell-free supernatants ($100\ \mu\text{g}$ of total protein/well; 12% SDS-PAGE under reducing conditions) Cat S was immunodetected by anti-Cat S primary antibody incubated overnight at 4°C . Horseradish peroxidase (HRP)-conjugated anti-IgG antibody was incubated for 1 h at room temperature, and immune-positive bands were visualized using an enhanced chemiluminescence assay kit (ECL Plus Western blotting detection system; Amersham Biosciences, UK). In addition, western-blot detection of STAT-3, phospho-STAT-3, and β -actin were performed in RHS. Following one-hour incubation of NHEK supernatants ($30\ \mu\text{g}$ of total protein) and RHS supernatants ($100\ \mu\text{g}$ of total protein) in 100 mM Hepes buffer, pH 7.4, 10 mM DTT, and 0.01% Brij35 at 37°C , Cat S activity was monitored using Z-LR-AMC ($30\ \mu\text{M}$). Specific activity of Cat S was checked using the inhibitor LHVS ($10\ \text{nM}$) as reported elsewhere [49].

Statistical analysis

Data were expressed as median \pm SD unless indicated and analyzed by non-parametric Mann-

Whitney U test. Statistical analysis was performed using GraphPad Prism (GraphPad software, San Diego, CA, USA). Differences at a p-value < 0.05 were considered significant.

Author contributions

FL supervised research; JS, EL, SAS, RK, GL, and FL designed research; JR, JS, EL, RD, KKB, AS, and TC performed research; RK, CN, and FL contributed new reagents; JR, JS, RK, SAS, GL, and FL analyzed data; FL wrote the paper. JS, RK, SAS, and GL revised the paper. All authors approved the final version of the manuscript mmc1.docx

Declaration of interests

The authors declare that they have no competing interests.

Acknowledgments

This work was supported by LVMH Recherche (Saint Jean de Braye, France) and by institutional funding from the Institut National de la Santé et de la Recherche Médicale (INSERM) and the University of Tours. TC held a doctoral fellowship from MESRI (Ministère de l'Enseignement Supérieur, de la Recherche et de l'Innovation, France). KKB held a BMN (Badania Młodych Naukowców) grant from the Faculty of Chemistry, University of Gdańsk (BMN-538-8370-B249-18) and a grant (UMO-2018/31/N/ST4/01677) from the National Science Centre of Poland (Narodowe Centrum Nauki). SAS received funding (grant UMO-2018/30/E/ST4/00037) from the National Science Centre of Poland (Narodowe Centrum Nauki). We are grateful to Maïlys Gaudet and Titouan Lescop for their technical help with keratinocytes and RHS experiments. Authors acknowledge Dr. Fabrice Gouilleux (Groupe Innovation et Ciblage Cellulaire, University of Tours, France) for providing STAT3 and pSTAT3 antibodies.

Received 14 December 2021;

Received in revised form 7 February 2022;

Accepted 9 February 2022

Available online 12 February 2022

Keywords:

Basement membrane;
Epidermis;
Extracellular-matrix;
Inhibition;
Keratinocyte;
Flavonoid;
Nidogen;
Protease

Abbreviations:

AEBSF, 4-(2-aminoethyl) benzenesulfonyl fluoride hydrochloride; BM, basement membrane; CA-074, N-(L-3-trans-propylcarbamoyloxirane-2-carbonyl)-L-isoleucyl-L-proline; Cat, cathepsin; EGCG, epigallocatechin 3-gallate; ECM, extracellular-matrix; LHVS, Morpholinourea-leucinyll-homophenylalanine-vinyl-sulfone; MMP, matrix metalloproteinase; MMTS, S-Methyl thiomethanesulfonate; NHDC, neohesperidin dihydrochalcone; NHP, neohesperidin; NSP, neutrophil serine proteases; NHEK, normal human epidermal keratinocytes; PMSF, phenylmethylsulfonyl fluoride; RHS, reconstructed human skin

*Authors contributed equally to this manuscript.

References

- [1] R.D.A. Wilkinson, R. Williams, C.J. Scott, R.E. Burden, Cathepsin S: therapeutic, diagnostic, and prognostic potential, *Biol. Chem.* 396 (2015) 867–882, doi: [10.1515/hsz-2015-0114](https://doi.org/10.1515/hsz-2015-0114).
- [2] H. Kirschke, B. Wiederanders, D. Brömme, A. Rinne, Cathepsin S from bovine spleen. Purification, distribution, intracellular localization and action on proteins, *Biochem. J.* 264 (1989) 467–473, doi: [10.1042/bj2640467](https://doi.org/10.1042/bj2640467).
- [3] G.P. Shi, J.S. Munger, J.P. Meara, D.H. Rich, H.A. Chapman, Molecular cloning and expression of human alveolar macrophage cathepsin S, an elastolytic cysteine protease, *J. Biol. Chem.* 267 (1992) 7258–7262.
- [4] A. Punturieri, S. Filippov, E. Allen, I. Caras, R. Murray, V. Reddy, S.J. Weiss, Regulation of elastolytic cysteine proteinase activity in normal and cathepsin K-deficient human macrophages, *J. Exp. Med.* 192 (2000) 789–799.
- [5] V.Y. Reddy, Q.Y. Zhang, S.J. Weiss, Pericellular mobilization of the tissue-destructive cysteine proteinases, cathepsins B, L, and S, by human monocyte-derived macrophages, *Proc. Natl. Acad. Sci. U. S. A.* 92 (1995) 3849–3853, doi: [10.1073/pnas.92.9.3849](https://doi.org/10.1073/pnas.92.9.3849).
- [6] D.Q. Yang, S. Feng, W. Chen, H. Zhao, C. Paulson, Y.-P. Li, V-ATPase subunit ATP6AP1 (Ac45) regulates osteoclast differentiation, extracellular acidification, lysosomal trafficking, and protease exocytosis in osteoclast-mediated bone resorption, *J. Bone Miner. Res.* 27 (2012) 1695–1707, doi: [10.1002/jbmr.1623](https://doi.org/10.1002/jbmr.1623).
- [7] M.M. Mohamed, B.F. Sloane, Cysteine cathepsins: multifunctional enzymes in cancer, *Nat. Rev. Cancer.* 6 (2006) 764–775.
- [8] H.A. Chapman, R.J. Riese, G.P. Shi, Emerging roles for cysteine proteases in human biology, *Annu. Rev. Physiol.* 59 (1997) 63–88, doi: [10.1146/annurev.physiol.59.1.63](https://doi.org/10.1146/annurev.physiol.59.1.63).
- [9] G.P. Shi, J.A. Villadangos, G. Dranoff, C. Small, L. Gu, K.J. Haley, R. Riese, H.L. Ploegh, H.A. Chapman, Cathepsin S required for normal MHC class II peptide loading and germinal center development, *Immunity* 10 (1999) 197–206, doi: [10.1016/s1074-7613\(00\)80020-5](https://doi.org/10.1016/s1074-7613(00)80020-5).
- [10] J. Sage, E. Leblanc-Noblesse, C. Nizard, T. Sasaki, S. Schnebert, E. Perrier, R. Kurfurst, D. Brömme, G. Lalmanach, F. Lecaille, Cleavage of nidogen-1 by cathepsin S impairs its binding to basement membrane partners, *PLoS One* 7 (2012) e43494, doi: [10.1371/journal.pone.0043494](https://doi.org/10.1371/journal.pone.0043494).
- [11] E. Vidak, U. Javoršek, M. Vizovišek, B. Turk, Cysteine cathepsins and their extracellular roles: shaping the microenvironment, *Cells* 8 (2019) E264, doi: [10.3390/cells8030264](https://doi.org/10.3390/cells8030264).
- [12] M. Vizovišek, E. Vidak, U. Javoršek, G. Mikhaylov, A. Bratovš, B. Turk, Cysteine cathepsins as therapeutic targets in inflammatory diseases, *Expert Opin. Ther. Targets* 24 (2020) 573–588, doi: [10.1080/14728222.2020.1746765](https://doi.org/10.1080/14728222.2020.1746765).
- [13] G. Schwarz, W.-H. Boehncke, M. Braun, C.J. Schröter, T. Burster, T. Flad, D. Dressel, E. Weber, H. Schmid, H. Kalbacher, Cathepsin S activity is detectable in human keratinocytes and is selectively upregulated upon stimulation with interferon-gamma, *J. Invest. Dermatol.* 119 (2002) 44–49, doi: [10.1046/j.1523-1747.2002.01800.x](https://doi.org/10.1046/j.1523-1747.2002.01800.x).
- [14] G.-P. Shi, G.K. Sukhova, M. Kuzuya, Q. Ye, J. Du, Y. Zhang, J.-H. Pan, M.L. Lu, X.W. Cheng, A. Iguchi, S. Perrey, A.M.-E. Lee, H.A. Chapman, P. Libby, Deficiency of the cysteine protease cathepsin S impairs microvessel growth, *Circ. Res.* 92 (2003) 493–500, doi: [10.1161/01.RES.0000060485.20318.96](https://doi.org/10.1161/01.RES.0000060485.20318.96).
- [15] J.A. Joyce, A. Baruch, K. Chehade, N. Meyer-Morse, E. Giraudo, F.-Y. Tsai, D.C. Greenbaum, J.H. Hager, M. Bogyo, D. Hanahan, Cathepsin cysteine proteases are effectors of invasive growth and angiogenesis during multistage tumorigenesis, *Cancer Cell* 5 (2004) 443–453, doi: [10.1016/s1535-6108\(04\)00111-4](https://doi.org/10.1016/s1535-6108(04)00111-4).
- [16] A. Schönefuss, W. Wendt, B. Schattling, R. Schulten, K. Hoffmann, M. Stuecker, C. Tigges, H. Lübbert, C. Stichel, Upregulation of cathepsin S in psoriatic keratinocytes, *Exp. Dermatol.* 19 (2010) e80–e88, doi: [10.1111/j.1600-0625.2009.00990.x](https://doi.org/10.1111/j.1600-0625.2009.00990.x).
- [17] V.B. Reddy, S.G. Shimada, P. Sikand, R.H. Lamotte, E.A. Lerner, Cathepsin S elicits itch and signals via protease-activated receptors, *J. Invest. Dermatol.* 130 (2010) 1468–1470, doi: [10.1038/jid.2009.430](https://doi.org/10.1038/jid.2009.430).
- [18] N. Kim, K.B. Bae, M.O. Kim, D.H. Yu, H.J. Kim, H.S. Yuh, Y.R. Ji, S.J. Park, S. Kim, K.-H. Son, S.-J. Park, D. Yoon, D.-S. Lee, S. Lee, H.-S. Lee, T.-Y. Kim, Z.Y. Ryoo, Overexpression of cathepsin S induces chronic atopic dermatitis in mice, *J. Invest. Dermatol.* 132 (2012) 1169–1176, doi: [10.1038/jid.2011.404](https://doi.org/10.1038/jid.2011.404).
- [19] J.S. Ainscough, T. Macleod, D. McGonagle, R. Brakefield, J.M. Baron, A. Alase, M. Wittmann, M. Stacey, Cathepsin S is the major activator of the psoriasis-associated proinflammatory cytokine IL-36 γ , *Proc. Natl. Acad. Sci. U. S. A.* 114 (2017) E2748–E2757, doi: [10.1073/pnas.1620954114](https://doi.org/10.1073/pnas.1620954114).
- [20] K. Chung, T. Pitcher, A.D. Grant, E. Hewitt, E. Lindstrom, M. Malcangio, Cathepsin S acts via protease-activated receptor 2 to activate sensory neurons and induce itch-like behaviour, *Neurobiol. Pain* 6 (2019) 100032, doi: [10.1016/j.nypai.2019.100032](https://doi.org/10.1016/j.nypai.2019.100032).

- [21] P. Panwar, T. Hedtke, A. Heinz, P.-M. Andraut, W. Hoehenwarter, D.J. Granville, C.E.H. Schmelzer, D. Brömme, Expression of elastolytic cathepsins in human skin and their involvement in age-dependent elastin degradation, *Biochim. Biophys. Acta Gen. Subj.* 1864 (2020) 129544, doi: [10.1016/j.bbagen.2020.129544](https://doi.org/10.1016/j.bbagen.2020.129544).
- [22] A.N. Panche, A.D. Diwan, S.R. Chandra, Flavonoids: an overview, *J. Nutr. Sci.* 5 (2016) e47, doi: [10.1017/jns.2016.41](https://doi.org/10.1017/jns.2016.41).
- [23] A. Vidal-Albalat, F.V. González, Atta-ur Rahman, Chapter 6 - Natural Products as Cathepsin Inhibitors, *Studies in Natural Products Chemistry*, Elsevier, 2016, pp. 179–213, doi: [10.1016/B978-0-444-63749-9.00006-2](https://doi.org/10.1016/B978-0-444-63749-9.00006-2).
- [24] W.-H. Boehncke, F. Ochsendorf, I. Paeslack, R. Kaufmann, T.M. Zollner, *Decorative cosmetics improve the quality of life in patients with disfiguring skin diseases*, *Eur. J. Dermatol.* 12 (2002) 577–580.
- [25] J. Sage, D. De Queral, E. Leblanc-Noblesse, R. Kurfurst, S. Schnebert, E. Perrier, C. Nizard, G. Lalmanach, F. Lecaille, Differential expression of cathepsins K, S and V between young and aged Caucasian women skin epidermis, *Matrix Biol.* 33 (2014) 41–46, doi: [10.1016/j.matbio.2013.07.002](https://doi.org/10.1016/j.matbio.2013.07.002).
- [26] K. Schueller, J. Hans, S. Pfeiffer, J. Walker, J.P. Ley, V. Somoza, Identification of Interleukin-8-Reducing Lead Compounds Based on SAR Studies on Dihydrochalcone-Related Compounds in Human Gingival Fibroblasts (HGF-1 cells) In Vitro, *Molecules* 25 (2020) E1382, doi: [10.3390/molecules25061382](https://doi.org/10.3390/molecules25061382).
- [27] G.E. Han, H.-T. Kang, S. Chung, C. Lim, J.A. Linton, J.-H. Lee, W. Kim, S.-H. Kim, J.H. Lee, Novel Neohesperidin Dihydrochalcone Analogue Inhibits Adipogenic Differentiation of Human Adipose-Derived Stem Cells through the Nrf2 Pathway, *Int. J. Mol. Sci.* 19 (2018) E2215, doi: [10.3390/ijms19082215](https://doi.org/10.3390/ijms19082215).
- [28] E.-R. Lee, Y.-J. Kang, J.-H. Kim, H.T. Lee, S.-G. Cho, Modulation of apoptosis in HaCaT keratinocytes via differential regulation of ERK signaling pathway by flavonoids, *J. Biol. Chem.* 280 (2005) 31498–31507, doi: [10.1074/jbc.M505537200](https://doi.org/10.1074/jbc.M505537200).
- [29] M. Matsuo, N. Sasaki, K. Saga, T. Kaneko, Cytotoxicity of flavonoids toward cultured normal human cells, *Biol. Pharm. Bull.* 28 (2005) 253–259, doi: [10.1248/bpb.28.253](https://doi.org/10.1248/bpb.28.253).
- [30] E. Noblesse, V. Cenizo, C. Bouez, A. Borel, C. Gleyzal, S. Peyrol, M.-P. Jacob, P. Sommer, O. Damour, Lysyl oxidase-like and lysyl oxidase are present in the dermis and epidermis of a skin equivalent and in human skin and are associated to elastic fibers, *J. Invest. Dermatol.* 122 (2004) 621–630, doi: [10.1111/j.0022-202X.2004.22330.x](https://doi.org/10.1111/j.0022-202X.2004.22330.x).
- [31] S. Choi, S. Yu, J. Lee, W. Kim, Effects of Neohesperidin Dihydrochalcone (NHDC) on Oxidative Phosphorylation, Cytokine Production, and Lipid Deposition, *Foods* 10 (2021) 1408, doi: [10.3390/foods10061408](https://doi.org/10.3390/foods10061408).
- [32] M. Comalada, I. Ballester, E. Bailón, S. Sierra, J. Xaus, J. Gálvez, F.S. de Medina, A. Zarzuelo, Inhibition of pro-inflammatory markers in primary bone marrow-derived mouse macrophages by naturally occurring flavonoids: analysis of the structure-activity relationship, *Biochem. Pharmacol.* 72 (2006) 1010–1021, doi: [10.1016/j.bcp.2006.07.016](https://doi.org/10.1016/j.bcp.2006.07.016).
- [33] S. Crouvezier, B. Powell, D. Keir, P. Yaqoob, The effects of phenolic components of tea on the production of pro- and anti-inflammatory cytokines by human leukocytes in vitro, *Cytokine* 13 (2001) 280–286, doi: [10.1006/cyto.2000.0837](https://doi.org/10.1006/cyto.2000.0837).
- [34] Q. Shi, X. Song, J. Fu, C. Su, X. Xia, E. Song, Y. Song, Artificial sweetener neohesperidin dihydrochalcone showed antioxidative, anti-inflammatory and anti-apoptosis effects against paraquat-induced liver injury in mice, *Int. Immunopharmacol.* 29 (2015) 722–729, doi: [10.1016/j.intimp.2015.09.003](https://doi.org/10.1016/j.intimp.2015.09.003).
- [35] P. Geraghty, C.M. Greene, M. O'Mahony, S.J. O'Neill, C.C. Taggart, N.G. McElvaney, Secretory leucocyte protease inhibitor inhibits interferon-gamma-induced cathepsin S expression, *J. Biol. Chem.* 282 (2007) 33389–33395, doi: [10.1074/jbc.M706884200](https://doi.org/10.1074/jbc.M706884200).
- [36] L.L.Y. Chan, B.K.W. Cheung, J.C.B. Li, A.S.Y. Lau, A role for STAT3 and cathepsin S in IL-10 down-regulation of IFN-gamma-induced MHC class II molecule on primary human blood macrophages, *J. Leukoc. Biol.* 88 (2010) 303–311, doi: [10.1189/jlb.1009659](https://doi.org/10.1189/jlb.1009659).
- [37] N. Fuchs, M. Meta, D. Schuppan, L. Nuhn, T. Schirmeister, Novel Opportunities for Cathepsin S Inhibitors in Cancer Immunotherapy by Nanocarrier-Mediated Delivery, *Cells* 9 (2020) E2021, doi: [10.3390/cells9092021](https://doi.org/10.3390/cells9092021).
- [38] D.H. Waalkens-Berendsen, M.E.M. Kuilman-Wahls, A. Bär, Embryotoxicity and teratogenicity study with neohesperidin dihydrochalcone in rats, *Regul. Toxicol. Pharmacol.* 40 (2004) 74–79, doi: [10.1016/j.yrtph.2004.05.007](https://doi.org/10.1016/j.yrtph.2004.05.007).
- [39] B.A. Lina, H.C. Dreef-van der Meulen, D.C. Leegwater, Subchronic (13-week) oral toxicity of neohesperidin dihydrochalcone in rats, *Food Chem. Toxicol.* 28 (1990) 507–513, doi: [10.1016/0278-6915\(90\)90121-3](https://doi.org/10.1016/0278-6915(90)90121-3).
- [40] A. Rodríguez, P. Webster, J. Ortego, N.W. Andrews, Lysosomes behave as Ca²⁺-regulated exocytic vesicles in fibroblasts and epithelial cells, *J. Cell Biol.* 137 (1997) 93–104, doi: [10.1083/jcb.137.1.93](https://doi.org/10.1083/jcb.137.1.93).
- [41] M. Ontiveros, D. Rinaldi, M. Marder, M.V. Espelt, I. Mangialavori, M. Vigil, J.P. Rossi, M. Ferreira-Gomes, Natural flavonoids inhibit the plasma membrane Ca²⁺-ATPase, *Biochem. Pharmacol.* 166 (2019) 1–11, doi: [10.1016/j.bcp.2019.05.004](https://doi.org/10.1016/j.bcp.2019.05.004).
- [42] C.J. Linnevers, M.E. McGrath, R. Armstrong, F.R. Mistry, M.G. Barnes, J.L. Klaus, J.T. Palmer, B.A. Katz, D. Brömme, Expression of human cathepsin K in *Pichia pastoris* and preliminary crystallographic studies of an inhibitor complex, *Protein Sci.* 6 (1997) 919–921, doi: [10.1002/pro.5560060421](https://doi.org/10.1002/pro.5560060421).
- [43] M.D. Hanwell, D.E. Curtis, D.C. Lonie, T. Vandermeersch, E. Zurek, G.R. Hutchison, Avogadro: an advanced semantic chemical editor, visualization, and analysis platform, *J. Cheminform.* 4 (2012) 17, doi: [10.1186/1758-2946-4-17](https://doi.org/10.1186/1758-2946-4-17).
- [44] O. Trott, A.J. Olson, AutoDock Vina: improving the speed and accuracy of docking with a new scoring function, efficient optimization and multithreading, *J. Comput. Chem.* 31 (2010) 455–461, doi: [10.1002/jcc.21334](https://doi.org/10.1002/jcc.21334).
- [45] D.A. Case, R.M. Betz, D.S. Cerutti, T.E. Cheatham, T.A. Darden, R.E. Duke, T.J. Giese, H. Gohlke, A.W. Goetz, N. Homeyer, S. Izadi, P. Janowski, J. Kaus, A. Kovalenko, T.S. Lee, S. LeGrand, P. Li, C. Lin, T. Luchko, R. Luo, B. Madej, D. Mermelstein, K.M. Merz, G. Monard, H. Nguyen, H.T. Nguyen, Y. Omelyan, A. Onufriev, D.R. Roe, A. Roitberg, C. Sagui, C.L. Simmerling, W.M. Botello-Smith, J. Swails, R.C. Walker, J. Wang, R.M. Wolf, X. Wu, L. Xiao, P.A. Kollman, 2016. doi:<https://doi.org/10.13140/RG.2.2.27958.70729>.
- [46] C. Dietz, M.R. Berthold, KNIME for Open-Source Bioimage Analysis: A Tutorial, *Adv. Anat. Embryol. Cell Biol.* 219 (2016) 179–197, doi: [10.1007/978-3-319-28549-8_7](https://doi.org/10.1007/978-3-319-28549-8_7).
- [47] F. Lecaille, T. Chazeirat, K.K. Bojarski, J. Renault, A. Saidi, V.G.N.V. Prasad, S. Samsonov, G. Lalmanach, Rat cathepsin K: Enzymatic specificity and regulation of its collagenolytic activity, *Biochim. Biophys. Acta Proteins Proteom.* 1868 (2020) 140318, doi: [10.1016/j.bbapap.2019.140318](https://doi.org/10.1016/j.bbapap.2019.140318).

- [48] T. Zuliani, V. Denis, E. Noblesse, S. Schnebert, P. Andre, M. Dumas, M.-H. Ratinaud, Hydrogen peroxide-induced cell death in normal human keratinocytes is differentiation dependent, *Free Radic. Biol. Med.* 38 (2005) 307–316, doi: [10.1016/j.freeradbiomed.2004.09.021](https://doi.org/10.1016/j.freeradbiomed.2004.09.021).
- [49] P.-M. Andrault, A.C. Schamberger, T. Chazeirat, D. Sizaret, J. Renault, C.A. Staab-Weijnitz, E. Hennen, A. Petit-Courty, M. Wartenberg, A. Saidi, T. Baranek, S. Guyetant, Y. Courty, O. Eickelberg, G. Lalmanach, F. Lecaille, Cigarette smoke induces overexpression of active human cathepsin S in lungs from current smokers with or without COPD, *Am. J. Physiol. Lung Cell. Mol. Physiol.* 317 (2019) L625–L638, doi: [10.1152/ajplung.00061.2019](https://doi.org/10.1152/ajplung.00061.2019).